

Ultraviolet–Visible Spectroelectrochemistry of Chemisorbed Molecular Layers on Optically Transparent Carbon Electrodes

HONG TIAN, ADAM JOHAN BERGREN, and RICHARD L. McCREERY*

Department of Chemistry, The Ohio State University, 100 W 18th Avenue, Columbus, Ohio 43210 (H.T.); and Department of Chemistry and National Institute for Nanotechnology, University of Alberta, Edmonton, Alberta, Canada T6G 2M9 (A.J.B., R.L.M.)

Pyrolysis of diluted commercial photoresist spun onto quartz slides yields optically transparent graphitic films. Transparent carbon electrodes ~6 nm thick can be reproducibly prepared, with a maximum absorbance in the ultraviolet–visible (UV-vis) range of 0.25 at 270 nm. These electrodes are sufficiently conductive for electrochemistry, enabling modification of the surface via diazonium ion reduction and spectroelectrochemistry. Good quality ultraviolet–visible absorption spectra of covalently bonded molecular layers of nitroazobenzene, nitrobiphenyl, and azobenzene, with thicknesses of 1.4–4 nm, were obtained after subtracting the spectrum of the unmodified substrate. The spectra of all three molecules immobilized on the carbon surface showed red shifts of the absorption maxima relative to a solution of free molecules, indicating substantial electronic interactions between chemisorbed molecules and the π system of the substrate and/or intermolecular coupling. Spectroelectrochemical measurements show that reduction of free and chemisorbed molecules produce new absorption features in the 500–800 nm range; these spectral changes are partially reversible upon repeated potential cycling. Finally, density functional calculations correlate the new bands to the formation of anion radical or “methide” species that have more extensive electron delocalization than the parent molecules. The results from this work are useful for linking structural transformations in molecular layers “buried” under conductive top contacts in a type of molecular junction to changes in the electronic properties of the junction.

Index Headings: Ultraviolet–visible spectroscopy; Spectroelectrochemistry; Thin films on carbon; Molecular electronics.

INTRODUCTION

Molecular electronics has been the focus of intense research over the past decade.^{1–11} A critical issue has been delineating the nature of electronic coupling between conducting “contacts” and the molecules under study as electronic components.^{12,13} Although many interesting and potentially valuable electronic phenomena have been reported for molecule-based devices, including nonlinear resistance,^{14,15} conductance switching,¹⁶ memory,^{9,17,18} and negative differential resistance,^{19,20} all rely on making contact between a conductor or semiconductor and molecules. Moreover, the importance of the contacts in determining the behavior of these devices is a topic of some controversy. For example, a gold/benzenedithiol/gold molecular junction has conductance properties that depend (at least) on junction structure, the energy levels of the benzene ring, and the facility of electron transfer from the gold contacts through the sulfur/Au bonds.^{14,21–25} Consequently, to meet the objective of exploiting the wide variety of electronic structures available from organic molecules as circuit components to achieve improved and/or novel microelectronic functions (one of the primary goals of molecular electronics), the coupling between conductors and molecules must be understood and,

ideally, controlled.^{12,26–28} To meet these goals, a robust and reproducible junction format is needed that can be used to establish relationships between electronic and molecular structure using a variety of analytical techniques.

Our group has recently reported several molecular electronic junctions based on covalent bonding between conducting carbon surfaces and aromatic molecules such as biphenyl, nitroazobenzene, fluorene, and nitrobiphenyl.^{15,29} These junctions exhibit electron transport properties that depend strongly on molecular structure, and in some cases exhibit phenomenon such as hysteresis and bistability, which might be employed in the development of molecular memory devices.^{9,30–32} In order to probe junction structure with optical spectroscopy, these junctions can be made with thin metal (or metal oxide) films as top contacts that are sufficiently conductive to enable the application of a bias voltage, and yet also are optically transparent.

Optical spectroscopy in all of its forms has been invaluable for characterizing molecular films adsorbed at solid surfaces. In particular, it is often the primary goal of an experiment to deduce the chemical or physical behavior of a molecular layer in response to an external stimulus (e.g., an applied voltage bias). Such characterizations are valuable for applications in many fundamental research areas, including electrochemistry, nanotribology, adhesion, and catalysis, and in the construction of chemical and biological sensors.^{33–36} Vibrational or electronic spectroelectrochemistry can provide dynamic structural and/or electron transfer mechanistic information.^{35,37–40} Changes in spectral features can be related to the corresponding transformations in the properties of a molecule resulting from oxidation or reduction at an electrode surface.

In this work we report spectroelectrochemistry of molecules both in solution and chemisorbed onto transparent carbon electrodes. Ultraviolet–visible (UV-vis) spectra for 1.4 to 4 nm thick layers of nitroazobenzene (NAB), azobenzene (AB), and nitrobiphenyl (NBP) chemisorbed on transparent carbon surfaces are obtained with a conventional spectrometer in air and also in electrolyte solution under potential control. Spectral changes as a function of applied potential are related to density functional theory (DFT) calculations for the reactants and structures related to possible reduction products. Collectively, the insights provided by this work provide a foundation for characterizing and tracking electronic levels in the devices, which serves as a strong complement to our previous Raman characterizations of structural changes for similar molecules in solid-state molecular electronics junctions.^{13,30,41–43} Moreover, the possibility of electronic coupling between the conductive “contacts” and the molecular layers adjacent to them is discussed.¹

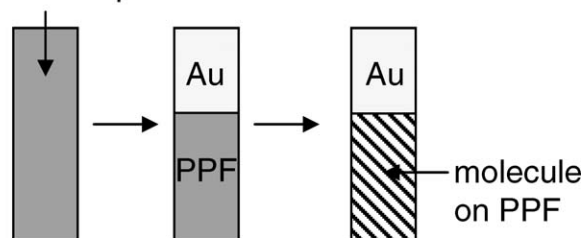
The work described herein was enabled by a recently developed protocol for preparing transparent carbon film electrodes described by Donner et al.⁴⁴ This technique provides

Received 29 June 2007; accepted 20 August 2007.

* Author to whom correspondence should be sent. E-mail: richard.mccreery@ualberta.ca.

Design 1

OTPPF on quartz



Design 2

OTPPF on quartz

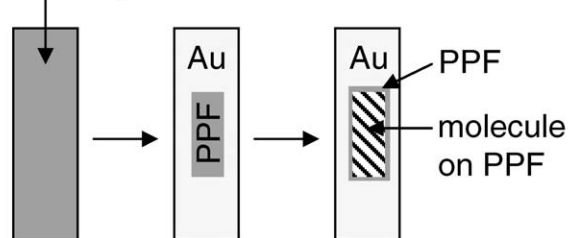


FIG. 1. Schematics of OTPPF on quartz: Design 1 (*top*) utilized a gold area adjacent to the OTPPF, while design 2 (*bottom*) tested a gold border surrounding the OTPPF to reduce ohmic potential errors. The hashed regions indicate the area intended for modification with diazonium reduction. Other materials as indicated.

a substrate that is suitable for optical absorbance measurements (i.e., is transparent over the UV-vis range) and that is sufficiently conductive for spectroelectrochemistry.

EXPERIMENTAL

Substrates. Optically transparent pyrolyzed photoresist films (OTPPF) were prepared by the method of Donner et al.⁴⁴ First, AZ-P4330-RS photoresist (AZ Electronic Materials, Somerville, NJ) was diluted to a concentration of 5% (v/v) with propylene glycol methyl ether acetate as the solvent. Next, this solution was spin-coated onto quartz slides at 6000 rpm for 60 s. After soft baking at 90 °C for 10 min, samples were transferred to a tube furnace for pyrolysis. A 5% H₂ in N₂ gas mixture is kept flowing at 100 sccm throughout pyrolysis, where the temperature was ramped at 10 °C min⁻¹ up to 1000 °C and held for 1 hour.^{45,46} Finally, the samples were allowed to cool to room temperature (H₂/N₂ still flowing). Preparation of non-transparent “bulk” pyrolyzed photoresist films (PPF) utilized the same procedure with non-diluted photoresist.

The OTPPFs were characterized with Raman spectroscopy, atomic force microscopy (AFM), spectroscopic ellipsometry, and UV-vis absorbance. Ten Raman spectra obtained along a 1.8 mm line on the OTPPF surface showed minimal variation in shape and a consistent D/G peak intensity ratio, with an average value of 1.91 ± 0.06 , indicating strong similarities to “bulk” PPF⁴⁶ (i.e., the presence of ordered graphitic crystalline phases is similar to, but not identical to, that found in glassy carbon). Line scans performed with AFM along 5 μm of OTPPF showed a maximum peak-to-peak variation of ± 1 nm, and a root mean square (rms) roughness of 0.5 to 0.8 nm, consistent with previous characterizations of “bulk” PPF.^{45,46}

Deposition of Molecular Layers. The synthesis of 4'-

nitroazobenzene (NAB), 4-azobenzene (AB) and 4'-nitro-biphenyl (NBP) diazonium tetrafluoroborate salts was carried out from the corresponding amines as described in detail elsewhere.^{29,47} Electrochemical deposition of organic layers from the diazonium reagents was carried out using 1 mM solutions in acetonitrile with 0.1 M tetrabutylammonium tetrafluoroborate (TBABF₄) as the supporting electrolyte. Surface modification was carried out with four cyclic scans from +0.4 to -0.6 V versus Ag/Ag⁺ at a sweep rate of 0.2 V s⁻¹. Although the details of the deposition procedures have been reported in detail elsewhere,^{9,48} the use of very thin OTPPF as the substrate presents some unique challenges.

The relatively high resistance of OTPPF yielded significant ohmic potential losses, resulting in poor coverage of the bonded films. In order to overcome this difficulty, an Au film was deposited onto the OTPPF, as shown in Fig. 1. Two separate geometries were tested. Design 1 utilized a 10 nm thick Au film adjacent to the OTPPF, while design 2 involved deposition of the Au as a contiguous border around the area to be modified. The border was sputter coated around a 4 × 15 mm solid shadow mask to yield a 4 × 15 mm unmodified OTPPF area, which was slightly larger than the window needed for optical experiments. Following deposition, a special electrochemical cell that exposed the center 3 × 12 mm of the OTPPF area to electrolyte solution was used to deposit molecules. As will be discussed below, design 2 significantly reduced potential error by providing a low resistance current path during electrochemical modification, resulting in uniform, high-coverage films, from which acceptable UV-vis spectra could be obtained.

After surface modification (using design 2), the thickness of the molecular layers were determined by AFM “scratching” of a 500 × 500 nm trench, followed by line profiles through the scratched area, as described in detail elsewhere.⁴⁸ The molecular layer thicknesses so determined were NAB, 3.96 ± 0.68 nm; AB, 3.22 ± 0.59 nm; and NBP, 1.35 ± 0.29 nm. Since the molecular lengths of the three molecules range from 1.37 to 1.48 nm, the NAB and AB films are clearly multilayers, while the NBP film thickness is close to that expected for a monolayer. These results are in agreement with previous reports by several authors in which multilayer formation has been demonstrated for diazonium modification.^{48–51}

A sample of solid NAB physisorbed on quartz was prepared by drop-casting a dilute solution of NAB in ether. Nitroazobenzene reagent and the amine precursors for diazonium synthesis were obtained from Sigma-Aldrich, and used as received.

Spectroelectrochemistry. For spectroelectrochemical experiments, a Perkin Elmer Lambda 900 UV-vis spectrometer was employed. A Bioanalytical Systems Epsilon potentiostat was used to control the potential within a quartz cuvette in the sample chamber of the spectrometer. The cell was allowed to equilibrate at each applied potential for ~6 minutes before acquiring spectra.

Variable Angle Spectroscopic Ellipsometry. Bulk PPF (freshly prepared) and polished glassy carbon (GC-20, Tokai Carbon) samples were characterized using variable angle spectroscopic ellipsometry (J.A. Woollam VASE). Four incident angles (50°, 60°, 70°, and 80°) were used, with the spectroscopic resolution set at 5 nm. Data analysis employed a two-phase model (substrate and air), where the dispersion of

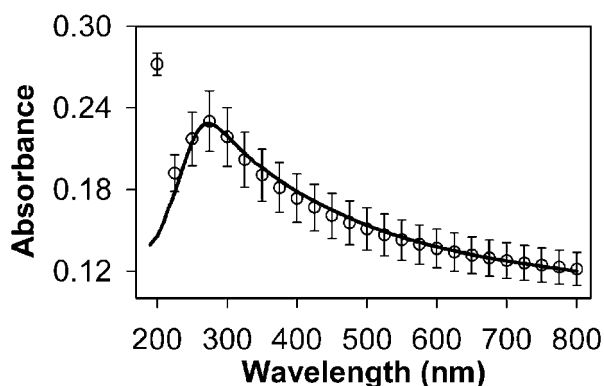


FIG. 2. Experimental absorbance spectrum of OTPPF (open circles) on quartz prepared using a 5% (v/v) solution of photoresist, with air as the reference. The error bars represent \pm one standard deviation for ten samples. The solid line is the calculated spectra using the optical constants for PPF determined with VASE (see Fig. 3) and a 4.8 nm thickness parameter (path length).

the optical constants of the substrates (PPF or GC) were modeled using a Cauchy function. Complex nonlinear least-squares fitting performed in the VASE32 software using this model resulted in fits for the optical constants (n and k), with mean-square errors (sum of the residual between experimental and modeled data for Ψ and Δ squared) of less than 0.9.

For thickness measurements of OTPPF, a three-phase model was used (quartz, OTPPF layer, and air). The values for n and k for quartz were preloaded in the VASE32 software (which uses literature values), while the OTPPF layer utilized fixed optical constants determined as described above. Since OTPPF on quartz is transparent, the data was analyzed in the back-side reflection-corrected mode in VASE32. The experimental values for Ψ and Δ (as a function of wavelength and angle of incidence) were fit to the thickness of the OTPPF layer. For all analyses of VASE data, the angles of incidence were corrected during the fitting algorithm (angles were accurate to $\pm 0.5^\circ$).

Theoretical Calculations. Gaussian '03 calculations for theoretical molecular layer lengths and HOMO-LUMO gaps were performed on a dual-Pentium PC with density functional theory (B3LYP) using a 6-31G(d) basis set.⁵² UV-vis spectra were simulated using Film Star (FTG software).

RESULTS AND DISCUSSION

Optical Properties of Optically Transparent Pyrolyzed Photoresist Films. Figure 2 shows the average experimental UV-vis spectrum obtained from ten OTPPF samples, with air as the reference. Error bars represent \pm one standard deviation, showing that the shape of the absorption profile is reproducible to within 10% in absorbance throughout this spectral region. The wavelength of maximum absorbance (λ_{\max}) varies less than 2% (272 ± 4 nm), while the absorbance value at λ_{\max} is 0.23 ± 0.02 (which corresponds to a minimum %T of $59 \pm 3\%$). The most likely cause of sample-to-sample variation in absorbance is small deviations in the thickness of the OTPPF when several samples are prepared under ostensibly identical conditions. To test this assertion, the thicknesses of the films were intentionally varied over a wide range by changing the concentration of the photoresist used to prepare the sample. In addition, UV-vis spectra were simulated as a function of film thickness using optical constants obtained from ellipsometric

TABLE I. Values for λ_{\max} , the transmission (%T) at λ_{\max} , and calculated thicknesses from spectral simulations as a function of photoresist dilution.

Photoresist dilution (v/v)	λ_{\max} (nm)		%T at λ_{\max}	Thickness (nm)	
	Experiment	Simulation		Simulation ^a	VASE
50%	257	256	0.04%	100	...
33%	260	260	2%	60	...
25%	265	265	26%	19.5	...
10%	270	268	37%	13	...
5%	272	274	57%	6.7	5.9 ± 0.8
1%	274	274	94%	0.25	...

^a Thickness producing the closest match of %T at λ_{\max} for a spectrum calculated from the optical constants shown in Fig. 3.

measurements. As shown in Table I, the values of λ_{\max} and film transmittance (%T) varied monotonically with the concentration of the photoresist, in agreement with the results of Donner et al.⁴⁴ For example, Donner et al. used a minimum photoresist concentration of 25% and observed $\sim 30\%$ T at 300 nm for a single coating, while we obtain $\sim 25\%$ T at 265 nm (see Table I), implying that the OTPPF samples are similar for the two labs. The small shift in λ_{\max} with thickness could arise from a number of causes, including differences in reflectivity and changes in the crystalline and/or electronic structure of the PPF. However, we do not currently understand the origin of this phenomenon.

In order to further characterize the optical properties of OTPPF, values for the refractive index (n) and extinction coefficient (k) of PPF and GC versus λ were determined using VASE. Figure 3 shows a plot of n and k as a function of wavelength for bulk PPF (open circles) and GC (filled circles). Also shown are literature values for GC (triangles).⁵³ Although the shapes of the curves are similar in all three cases, there are significant differences in magnitude over most of the spectral range examined. The differences between the literature values⁵³ for n and k and our results for GC is probably attributable to variations in surface roughness produced by hand polishing of the GC. On the other hand, the offsets in the data for PPF relative to GC may be due to the disparity of a number of factors, including, for example, surface roughness, the size and/or distribution of graphitic crystal grains, and the types and densities of functional groups at the surfaces of the two substrates. For all three substrates, Fig. 3 indicates the presence of an absorbance band at ~ 260 nm (i.e., the wavelength at which the derivative of n with respect to λ and the value of k are maximized), which is consistent with the experimental data shown in Fig. 2. Moreover, the data in Fig. 3 were used to calculate UV-vis spectra for thin layers of PPF or GC, which confirmed the presence of the absorbance band. The solid curve in Fig. 2 is a calculated spectrum for PPF using the optical constants in Fig. 3 and a thickness of 4.8 nm. The excellent correspondence with the observed spectrum indicates that the n and k values determined from ellipsometry are reliable, and also that PPF made with 5% photoresist solution is ~ 5 nm thick.

The thicknesses of PPF samples made from various dilutions of photoresist were estimated by simulating spectra using the optical constants of PPF. The thickness of the PPF layer was adjusted until the transmittance at λ_{\max} (or λ_{\min} in this case) in the calculated spectrum matched the experimental value (results listed in Table I). For the case of the 5% diluted sample, the thickness of the PPF was also determined using

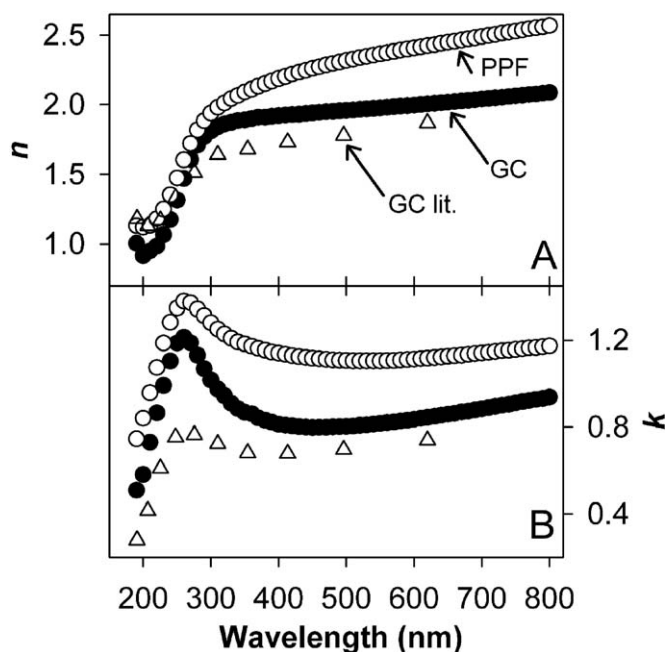


Fig. 3. Optical constants (A) n and (B) k for polished glassy carbon (GC) (solid circles), “bulk” (i.e., non-transparent) PPF (open circles), and literature values for GC⁵³ (open triangles) as a function of wavelength.

VASE. Both methods yield a thickness of ~ 6 nm, with approximately 10% standard deviation in the ellipsometric data (three samples). This level of variation shows that the deviation observed in the absorbance spectra for OTPPF can reasonably be explained by thickness effects (i.e., differences of 1–2 nm in film thickness). This fact is important when referencing spectra of molecules adsorbed on OTPPF, as discussed below.

Spectra of Molecules Chemisorbed on Optically Transparent Pyrolyzed Photoresist Films. Based on the optical characterization of OTPPF, samples prepared using a photoresist dilution of 5% (v/v) were chosen for spectroelectrochemistry due to the high transmittance of the samples (i.e., at least 57% over the range 220 to 800 nm), which maximizes spectroscopic sensitivity. Although the reproducibility of film absorbance at λ_{max} is reasonable (0.24 ± 0.03), it is too large to permit an accurate subtraction of a standard PPF absorption spectrum from those obtained for molecules bonded to PPF. Consequently, each OTPPF sample was used as its own “reference” for optical measurements by recording a spectrum before and after deposition of the molecular layer.

Figure 4A shows UV-vis spectra for OTPPF and NAB/OTPPF, with air as a reference. While the additional absorbance due to the thin molecular layer is apparent, it is more obvious after subtraction of the OTPPF spectrum from that for NAB/OTPPF (for the same OTPPF sample), as shown in Fig. 4B. Note that the subtraction accurately accounts for the absorbance of the OTPPF electrode since it is a self-referencing method, and therefore the band at ~ 270 nm does not contribute significantly to the spectra in Fig. 4B. The correction procedure also reduces the overall absorbance to a level that represents only the absorbance of the molecular layer. This process also reduces errors resulting from small differences in the OTPPF thickness, and perhaps other sample-to-sample variations causing the optical absorbance of each OTPPF substrate to fluctuate.

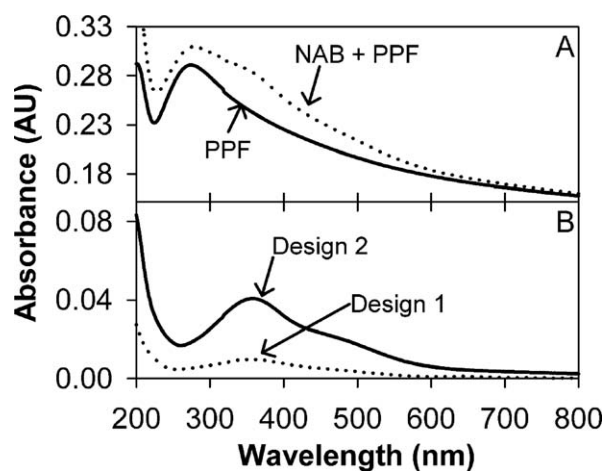


Fig. 4. (A) UV-vis absorption spectra of NAB/OTPPF/quartz (dotted curve), with air as a reference. The spectrum for the same OTPPF/quartz sample before bonding of NAB is also shown (solid curve). (B) Absorbance spectra of NAB on OTPPF obtained by subtracting the absorbance of NAB/OTPPF/quartz from that for the same OTPPF/quartz sample prior to modification. The dotted curve (design 1) is for deposition of the Au area adjacent to the OTPPF (see Fig. 1, top), while the solid curve (design 2) is for the Au border (see Fig. 1, bottom). Design 2 was used in panel (A).

As discussed above, the high resistivity of OTPPF necessitates particular attention to ohmic potential error when it is used as an electrode. The resistivity of PPF ($0.005 \Omega\text{-cm}$) is comparable to that of glassy carbon,⁴⁶ which is significantly higher than that for most metals. Based on this value, the predicted resistance for a 6 nm OTPPF electrode is $8.3 \times 10^3 \Omega/\text{m}$, illustrating that significant potential error can result during the electrochemical modification procedure such that the characteristics of the NAB films on OTPPF (i.e., thickness, packing density, etc.) may be affected. Figure 4B shows UV-vis spectra that were obtained using OTPPF electrodes modified with NAB using both of the designs shown in Fig. 1 (OTPPF was used as its own reference in both cases, as described above). Clearly, design 2 results in a higher density of absorbing species on the surface, indicating that without the Au border, ohmic potential losses lead to reduced NAB surface concentrations. Consequently, we have chosen design 2 in all further experiments to ensure a minimal variability in absorbance due to inefficient modification. As noted in the experimental section, design 2 yielded molecular layer thicknesses comparable to those obtained on bulk PPF. The results shown in Fig. 4 demonstrate that UV-vis spectra for molecules chemisorbed onto OTPPF can be obtained with sufficient signal to identify spectral features. However, it is worth noting that the relatively high resistance of OTPPF is a possible source of error whenever large electrochemical currents are required.

Free and Adsorbed Molecular Spectra. In order to establish the spectral signatures of the molecules and derive insight into the effect of covalent immobilization, spectra for molecules in solution are compared to that for the chemisorbed state. Figure 5 shows spectra of NAB in cyclohexane solution (5A), chemisorbed onto OTPPF (5B), and as a solid film (5C). The chemisorbed spectrum was obtained by subtracting the response for the same OTPPF/quartz sample prior to NAB modification from that for NAB/OTPPF/quartz. Figure 5B establishes that the absorbance spectra of thin layers of molecules bonded to OTPPF are readily measurable, giving

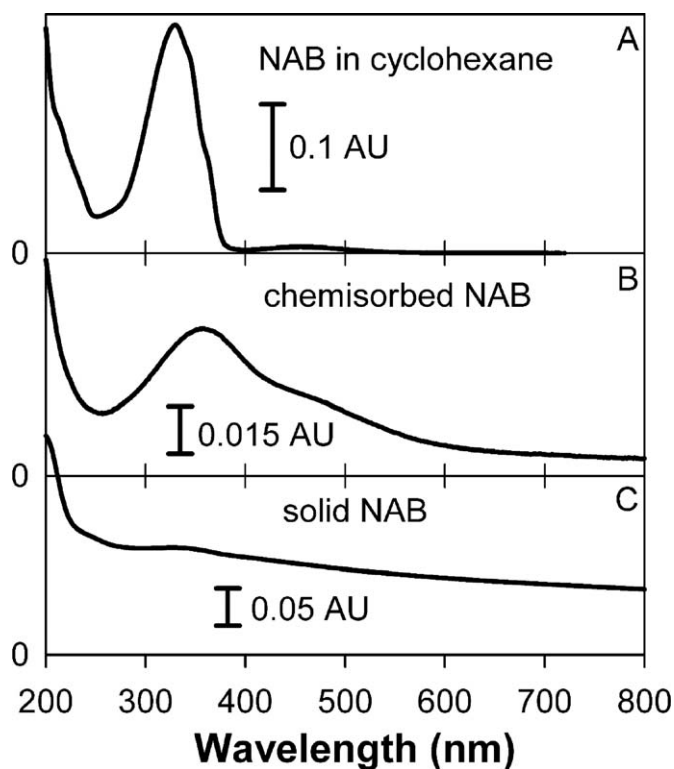


FIG. 5. UV-vis spectra of (A) 1×10^{-5} M NAB in cyclohexane, with cyclohexane as a reference; (B) chemisorbed NAB (4 nm thick) on OTPPF, obtained as described for Fig. 4B; and (C) solid NAB film on quartz, prepared by drop-casting from ether solution (unknown thickness).

signals in the range 0.02–0.05 absorbance units. These observations can be accounted for by considering the concentration and molar absorptivity of NAB in the thin film. The NAB film thickness and coverage determined previously (4.0 nm and 4×10^{-10} mol cm⁻², respectively)^{41,43} corresponds to a concentration of 0.001 mol cm⁻³. The molar absorptivity of NAB in cyclohexane is 28 000 M⁻¹ cm⁻¹ (see Fig. 5A), which leads to an estimated absorbance of 0.011 for a 4 nm path length (NAB thickness) after the application of Beer's law. Although the film spectrum is not expected to accurately correspond to that obtained in solution, the estimate shows that the peak absorbance of 0.031 in Fig. 5B is reasonable.

Several other important observations result from a comparison of the spectra in Fig. 5. First, chemisorbed NAB shows a main absorbance band that is both broadened and significantly red shifted with respect to NAB in cyclohexane. Second, there is significant absorbance out to at least 800 nm for chemisorbed NAB, whereas in solution the absorbance vanishes for λ greater than ~ 550 nm. Finally, the spectrum of solid NAB of unknown thickness (drop-cast from ether) also shows considerable absorbance across the visible range, with a weak peak at 334 nm.

Similar results to those shown in Fig. 5 for NAB were obtained for AB and NBP. Figure 6 shows spectra for AB and NBP in cyclohexane and chemisorbed on OTPPF. In both cases, the immobilized molecules show spectra that have red-shifted and broadened absorbance features, as was the case for NAB. However, the solid spectra for these two molecules (not shown) have more severely broadened features than that for NAB. Table II lists λ_{\max} for all three molecules in the

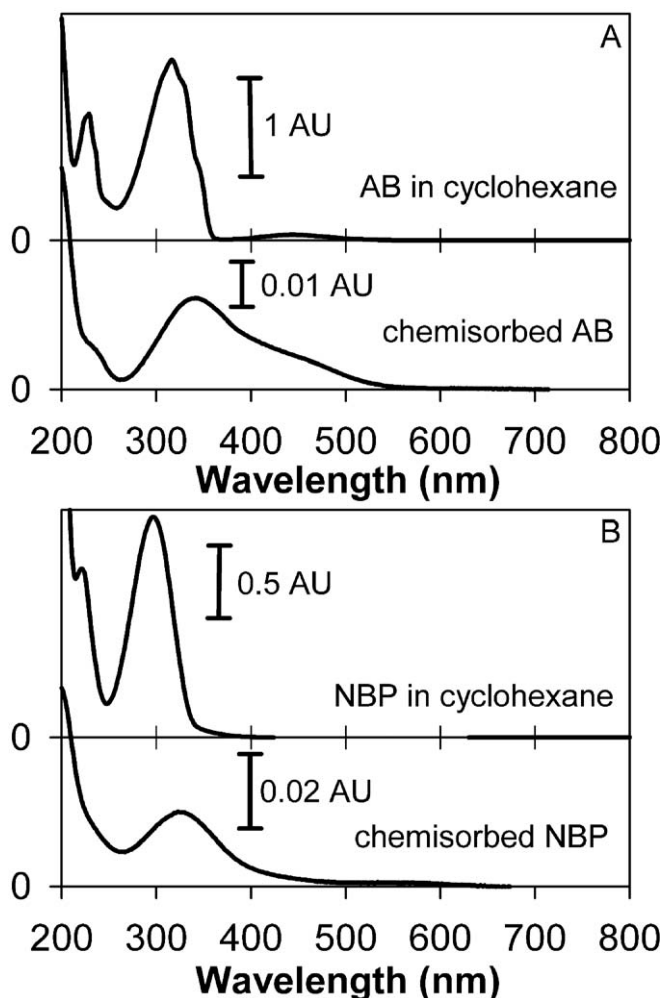


FIG. 6. UV-vis spectra of (A) (top) 1×10^{-4} M AB in cyclohexane, and (bottom) chemisorbed AB (3.2 nm thick) on OTPPF; and (B) (top) 1×10^{-4} M NBP in cyclohexane, and (bottom) chemisorbed NBP (1.4 nm thick) on OTPPF. Spectra obtained as described for Fig. 4B.

chemisorbed, solution, and solid states. Analysis of Table II shows a consistent trend: λ_{\max} is at a minimum in solution, highest for the chemisorbed films, and intermediate (although closer to the solution value) for the drop-cast film. Previous work for NAB chemisorbed at smooth silver surfaces also revealed a red shift in the chemisorbed spectrum, although the spectrum on Ag has a different shape from that on PPF.⁵⁴

The trends noted above can be caused by at least two effects. First, electronic coupling between the chemisorbed molecules and the graphitic π system may be substantial, resulting in changes in orbital energies that lead to decreases in the HOMO-LUMO gap. Second, intermolecular interactions

TABLE II. Observed λ_{\max} for chemisorbed, solution, and solid molecules.

Molecule	λ_{\max} , nm		
	Chemisorbed	Solution (in C ₆ H ₁₂)	Solid
NAB	356	330	336
AB	340	316	320
NBP	325	296	312

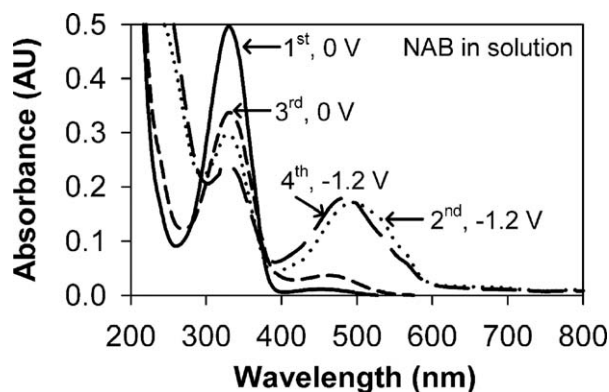


FIG. 7. UV-vis spectra for 1.0×10^{-4} M NAB dissolved in acetonitrile containing 0.1 M TBABF₄ obtained through an OTPPF electrode as a function of E_{appl} (vs. Ag/Ag⁺). Reference spectra collected at open circuit with no NAB. The optical path length in the solution was ~ 5 mm. Spectra were acquired ~ 6 minutes after E_{appl} was stepped, in the order indicated.

within the densely packed molecular film could cause a similar effect, or perhaps reinforce the effect of substrate coupling. Although the thicknesses of the drop-cast solid films are unknown, these samples were prepared as analogues to the chemisorbed film, but without covalent bond formation between the molecular film and substrate (or between molecules in the layer). The results in Figs. 5 and 6 and Table II establish essential features that will be used to analyze changes in spectral features in spectroelectrochemical experiments. These results will then be analyzed together with density functional calculations to investigate the possibility of electronic coupling effects.

Spectroelectrochemistry. Figure 7 shows UV-vis spectra of 0.1 mM NAB in acetonitrile (with 0.1 M TBABF₄ as supporting electrolyte) as a function of the potential applied (E_{appl}) to an OTPPF working electrode immersed in the solution. Spectra are referenced to OTPPF in blank electrolyte (no NAB) at open circuit. Comparison of Fig. 7 to Fig. 5A shows that the initial spectrum for NAB at $E_{\text{appl}} = 0$ V (vs. Ag/Ag⁺) is very similar to that for NAB in cyclohexane. At this potential, no NAB reduction should occur. However, when E_{appl} is stepped to -1.2 V, a potential at which reduction is expected to occur, a new absorption band appears between 490 and 500 nm, the absorbance above ~ 500 nm undergoes a general increase, and the original band at 330 nm decreases in magnitude. These spectral changes are at least partially reversible with repeated cycling between E_{appl} values of 0 and -1.2 V, indicating that the process leading to changes in the electronic spectrum of NAB is chemically reversible. As discussed in more detail below, we attribute the absorption band at 490–500 nm to the NAB anion formed upon reduction by one electron. AB and NBP in solution show similar trends upon reduction in acetonitrile, with the AB reduction product having a maximum absorption at 422 nm and the maximum absorption of reduced NBP at 560 nm. We note, however, that the full magnitude observed initially for a given band is not fully recovered upon returning E_{appl} from a reducing potential back to 0 V. Moreover, the degree of degradation was strongly dependent on the level of residual O₂ in the N₂-purged solution and sample chamber, possibly indicating that the reduction product of NAB is unstable in the presence of O₂ in solution.

Spectroelectrochemistry for Chemisorbed Nitroazobenzene. Figure 8 shows UV-vis spectra of an NAB-modified

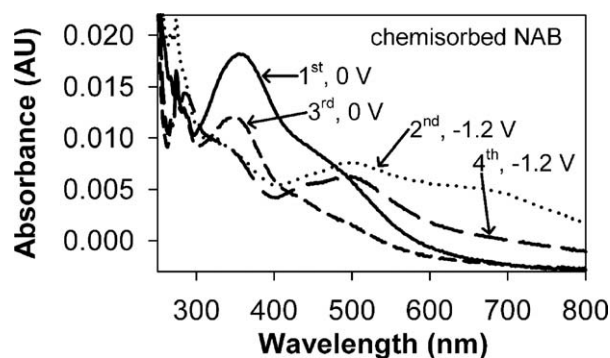


FIG. 8. Spectroelectrochemical sequence similar to that of Fig. 7, but for NAB chemisorbed on an OTPPF electrode immersed in blank 0.1 M TBABF₄ in acetonitrile. Spectra referenced to unmodified OTPPF immersed in the same solution.

OTPPF electrode immersed in 0.1 M TBABF₄ in acetonitrile. No NAB was present as a free molecule in solution, and the spectra are referenced to unmodified OTPPF in the same electrolyte solution. The initial spectrum at $E_{\text{appl}} = 0$ V in Fig. 8 has the same general appearance as the spectrum for chemisorbed NAB in air (see Fig. 4B); the long wavelength bands at ~ 360 and ~ 500 nm have roughly the same positions and shape. The spectra in Figs. 5B and 8 are not, however, identical. For example, there is additional absorbance between 250 and 300 nm that we attribute to the subtraction of the relatively large OTPPF/CH₃CN background. In an analogous fashion to the process described for Fig. 7, four spectra are shown in Fig. 8 collected for a sequence of E_{appl} values of 0, -1.2 , 0, and -1.2 V. When E_{appl} is stepped from 0 to -1.2 V, the band at ~ 360 nm decreases in intensity, an additional absorbance band at ~ 500 nm appears, and the absorbance above ~ 500 nm undergoes a general increase. These changes are qualitatively similar to those observed for NAB in solution (Fig. 7). Moreover, as observed for NAB in solution, the changes for chemisorbed NAB were partially reversible during a second potential cycle, with some degradation of the reduced form with time, possibly from interactions with water or oxygen. Collectively, the experiments in Figs. 7 and 8 demonstrate changes in the electronic properties of NAB for negative E_{appl} , both in solution and chemisorbed onto carbon. As discussed below, these trends are consistent with a one-electron reduction mechanism.

Theoretical Calculations. We have reported previously on the reduction of NAB to a radical anion⁴¹ and its relevance to the conductance changes observed in PPF/NAB/TiO₂ molecular junctions.⁴³ Based on Raman evidence, these earlier studies showed that chemisorbed NAB is reduced to a quinoid form at approximately -1 V (vs. Ag/Ag⁺) in acetonitrile. As shown in Table III and discussed in more detail below, the quinoid form of chemisorbed NAB is expected to have a smaller HOMO-LUMO gap (2.1 eV) relative to the parent molecule (3.6 eV), based on density functional theory calculations (Gaussian '03).⁴¹ Thus, using insights derived from calculated gap energies, the changes observed in electronic spectra as a function of E_{appl} can be related to structural models.

Figure 9 shows several relevant chemical structures. The top row shows NAB in three different forms: the free molecule (left) and two anions representing possible structures for reduced NAB (center and right). Of the two reduced forms,

TABLE III. Calculated HOMO-LUMO gaps for parent molecules and radicals.^a

Molecules	Gap (nm)		
	HOMO-LUMO	HOMO-SOMO	SOMO-LUMO
NAB			
Parent, planar	349.5		
Restricted radical anion	298.4	504.3	730.9
Methide anion	588.3		
AB			
Parent, planar	314.0		
Radical anion	241.2	565.7	420.6
Methide anion	488.1		
NBP			
Parent, 37° dihedral	291.7		
Radical anion, 21° dihedral	236.8	391.8	598.5
Methide anion, 1.1° dihedral	633.1		

^a Gaussian '03, B3LYP/6-31 G(d).⁵²

NAB in solution corresponds to the center radical anion structure, while a non-radical “methide” species at far right relates to reduced NAB chemisorbed at carbon. The “methide” linkage is a model structure for NAB chemisorbed to the edge plane of PPF, after a one electron reduction. The bottom row of Fig. 9 shows a corresponding series of structures for NBP.

Table III lists HOMO-LUMO gaps calculated for NAB, AB, and NBP and the two reduced species as in Fig. 9. Note that for the radical anions, two additional gaps are listed corresponding to electronic transitions from the fully occupied HOMO to the half-filled (i.e., sometimes occupied, SO) radical orbital (HOMO-SOMO) and one for the radical orbital to LUMO (SOMO-LUMO). Calculated dihedral angles between the two rings for NBP are also given in Table III (all three forms of NAB and AB are predicted to be planar). Note that the dihedral angle decreases upon reduction, with a nearly planar geometry for the methide anion. Most importantly, however, in all cases reduction produces long wavelength absorption band(s); in solution, these correspond to HOMO-SOMO or SOMO-LUMO transitions for the radical species, while the HOMO-LUMO gap for the reduced chemisorbed molecules red-shifts: NAB from 350 to 588 nm, AB from 314 to 488 nm, and NBP from 292 to 633 nm.

As discussed earlier, reduction of NAB in solution (Fig. 7) results in a significant decrease in the intensity of the absorbance band at ~330 nm, with concurrent increases in the absorbance below 200 nm and in bands at ~500 and ~550 nm. Referring to Table III, the changes in the electronic spectra are consistent with reduction of NAB to a radical anion, with a blue shift in the HOMO-LUMO gap (explaining the increased absorbance below 200) and more intensity at longer wavelengths due to HOMO-SOMO transitions.

As shown in Fig. 8, reduction of chemisorbed NAB produces similar results. The best matches to the transitions in Table III implicate the reduction of NAB to a radical anion or methide species. That is, the long wavelength absorption for reduced NAB indicates narrowing of the HOMO-LUMO gap (methide anion). The general red-shifted absorbance features for chemisorbed films relative to NAB in solution, combined with the much smaller red-shift for solid films, demonstrates that covalent bonding of molecules to aromatic carbon surfaces can result in structures with enhanced delocalization of

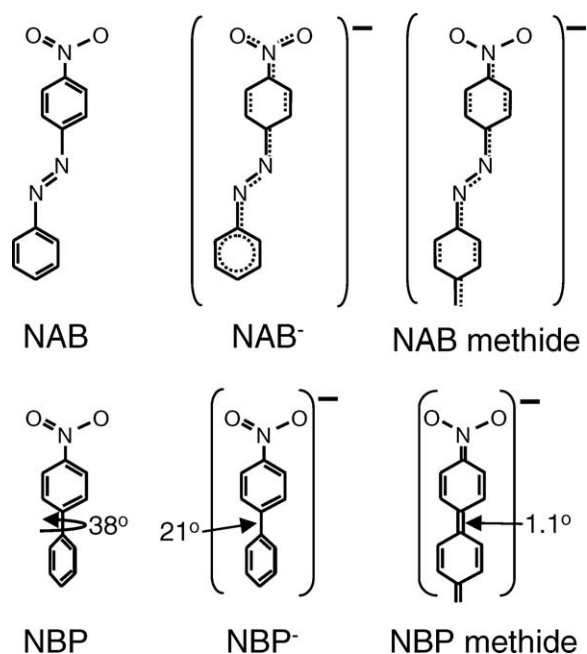


FIG. 9. Structures of (top row) NAB and (bottom row) NBP parent molecules (left), anions (center), and methide anions (right). The methide is a model for the parent molecule bonded to the edge plane of PPF, then reduced by one electron. Dihedral angles between phenyl rings are shown for NBP; the NAB and AB molecules are planar in all forms.

electrons relative to the free molecule. The reduction of chemisorbed molecules can augment this effect, showing that injection of electrons into films chemisorbed to carbon can lead to extensive electron delocalization, possibly providing a basis for conductance changes in electronic junctions.

CONCLUSION

Carbon is a less common optically transparent electrode (OTE) material used in spectroelectrochemistry,^{37,38} however, this work demonstrates that OTPPF can be effectively provided ohmic losses are acceptably low. Spectroelectrochemistry of organic nanofilms (i.e., monolayers or multilayers with <10 nm thickness) is typically reported for relatively thick films of strong absorbers^{55–57} or for films on high surface area structures such as supported nanoparticle arrays.^{58,59} However, as noted in the Introduction, the rapidly rising interest in molecular electronics provides a strong incentive to develop spectroscopic methods that can provide dynamic structural and electronic information about nanofilms.

The UV-vis method described herein may be particularly useful for studying molecular electronic devices composed of stratified components since the spectral changes are directly related to electronic structure. Thus, the approach may provide insights into electron transfer mechanisms occurring within the device under bias. UV-vis absorption spectroscopy provides information that is complementary to previously developed Raman techniques but also is likely to prove much more general since far more organic molecules are strong UV-vis absorbers than are strong Raman scatterers. For example, the reduction of NAB in molecular junctions was observed with Raman spectroscopy, but the technique relied on strong resonant Raman enhancement for adequate sensitivity. Nitro-biphenyl, fluorene, etc., do not have strong Raman cross-

sections but may be amenable to monitoring with UV-vis absorption. A partially transparent molecular junction of the type OTPPF/molecule/TiO₂/Au would permit absorption measurements on an active junction in response to changes in bias. We are currently pursuing work along these lines to probe the electronic and structural changes in devices with active regions in the thickness range of 2–10 nm.

ACKNOWLEDGMENTS

This work was supported by the National Science Foundation through project 0211693 from the Analytical and Surface Chemistry Division. Portions of this work were carried out at the University of Alberta Nanofab facility.

1. R. L. McCreery, *Anal. Chem.* **78**, 3490 (2006).
2. C. D. Lindstrom, M. Muntwiler, and X. Y. Zhu, *J. Phys. Chem. B* **109**, 21492 (2005).
3. A. S. Blum, J. G. Kushmerick, D. P. Long, C. H. Patterson, J. C. Yang, J. C. Henderson, Y. Yao, J. M. Tour, R. Shashidhar, and R. R. Ratna, *Nature Mater.* **4**, 167 (2005).
4. A. Flood, J. Stoddart, D. Steueman, and J. Heath, *Science (Washington, D.C.)* **306**, 2055 (2004).
5. T. Rakshit, G. Liang, A. Ghosh, and S. Datta, *Nano Lett.* **4**, 1803 (2004).
6. J. R. Heath and M. A. Ratner, *Phys. Today* **56**, 43 (2003).
7. C. Joachim, *Superlattices Microstruct.* **28**, 305 (2000).
8. J. Jortner and M. Ratner, *Molecular Electronics* (Blackwell Science Ltd., Oxford, 1997), 1st ed.
9. R. McCreery, J. Wu, and R. J. Kalakodimi, *Phys. Chem. Chem. Phys.* **8**, 2572 (2006).
10. M. Galperin, M. Ratner, and A. Nitzan, *Nano Lett.* **5**, 125 (2005).
11. R. McCreery, *Chem. Mater.* **16**, 4477 (2004).
12. V. Mujica and M. A. Ratner, *Chem. Phys.* **264**, 365 (2001).
13. R. L. McCreery, U. Viswanathan, R. P. Kalakodimi, and A. M. Nowak, *Faraday Discuss.* **131**, 33 (2006).
14. S. Howell, D. Kuila, B. Kasibhatla, C. P. Kubiak, D. Janes, and R. Reifenger, *Langmuir* **18**, 5120 (2002).
15. F. Anariba, J. Steach, and R. McCreery, *J. Phys. Chem. B* **109**, 11163 (2005).
16. Z. J. Donhauser, B. A. Mantooth, K. F. Kelly, L. A. Bumm, J. D. Monnell, J. J. Stapleton, D. W. Price, A. M. Rawlett, D. L. Allara, J. M. Tour, and P. S. Weiss, *Science (Washington, D.C.)* **292**, 2303 (2001).
17. J. C. Scott and L. D. Bozano, *Adv. Mater.* **19**, 1452 (2007).
18. J. Wu, K. Mobley, and R. McCreery, *J. Chem. Phys.* **126**, 24704 (2007).
19. Y. Xue, S. Datta, S. Hong, R. Reifenger, J. I. Henderson, and C. P. Kubiak, *Phys. Rev. B* **59**, R7852 (1999).
20. J. Chen, M. A. Reed, A. M. Rawlett, and J. M. Tour, *Science (Washington, D.C.)* **286**, 1550 (1999).
21. M. A. Reed, C. Zhou, C. J. Muller, T. P. Burgin, and J. M. Tour, *Science (Washington, D.C.)* **278**, 252 (1997).
22. J. Chen, L. C. Calvet, M. A. Reed, D. W. Carr, D. S. Grubisha, and D. W. Bennett, *Chem. Phys. Lett.* **313**, 741 (1999).
23. M. A. Reed and T. Lee, Eds. *Molecular Nanoelectronics* (American Scientific Publishers, Stevenson Ranch, 2003), 1st ed.
24. W. Tian, S. Datta, S. Hong, R. Reifenger, J. I. Henderson, and C. P. Kubiak, *J. Chem. Phys.* **109**, 2874 (1998).
25. S. Hong, R. Reifenger, W. Tian, S. Datta, J. Henderson, and C. P. Kubiak, *Superlattices Microstruct.* **28**, 289 (2000).
26. J. M. Seminario, C. E. De La Cruz, and P. A. Derosa, *J. Am. Chem. Soc.* **123**, 5616 (2001).
27. A. L. Burin and M. A. Ratner, *J. Phys. Chem.* **113**, 3941 (2000).
28. S. N. Yaliraki and M. A. Ratner, *J. Phys. Chem.* **109**, 5036 (1998).
29. F. Anariba and R. L. McCreery, *J. Phys. Chem. B* **106**, 10355 (2002).
30. A. Nowak and R. McCreery, *J. Am. Chem. Soc.* **126**, 16621 (2004).
31. R. McCreery, *Electrochem. Soc. Interface* **13**, 46 (2004).
32. R. L. McCreery, J. Dieringer, A. O. Solak, B. Snyder, A. Nowak, W. R. McGovern, and S. DuVall, *J. Am. Chem. Soc.* **125**, 10748 (2003).
33. A. J. Bard and L. R. Faulkner, *Electrochemical Methods* (John Wiley and Sons, New York, 2001), 2nd ed.
34. R. J. Gale, *Spectroelectrochemistry, Theory and Practice* (Plenum Press, New York, 1988), 1st ed.
35. W. R. Heineman, F. M. Hawkridge, and H. Blount, "Spectroelectrochemistry at Optically Transparent Electrodes. II. Electrodes Under Thin-Layer and Semi-Infinite Diffusion Conditions and Indirect Coulometric Titrations," in *Electroanalytical Chemistry*, A. J. Bard, Ed. (Marcel Dekker, New York, 1984), vol. 13.
36. R. L. McCreery, "Spectroelectrochemistry," in *Physical Methods in Chemistry*, B. Rossiter, Ed. (John Wiley and Sons, New York, 1986), vol. 2.
37. T. P. DeAngelis, R. W. Hurst, A. M. Yacynych, H. B. Mark, Jr., W. R. Heineman, and J. S. Mattson, *Anal. Chem.* **49**, 1395 (1977).
38. S. Haymond, J. K. Zak, Y. Show, J. E. Butler, G. T. Babcock, and G. Swain, *Anal. Chim. Acta* **500**, 137 (2003).
39. T. Kuwana and N. Winograd, "Spectroelectrochemistry at Optically Transparent Electrodes; I. Electrodes Under Semi-Infinite Diffusion Conditions," in *Electroanalytical Chemistry*, A. J. Bard, Ed. (Marcel Dekker, New York, 1974), vol. 7.
40. M. Petek, T. E. Neal, and R. W. Murray, *Anal. Chem.* **43**, 1069 (1971).
41. T. Itoh and R. L. McCreery, *J. Am. Chem. Soc.* **124**, 10894 (2002).
42. R. P. Kalakodimi, A. Nowak, and R. L. McCreery, *Chem. Mater.* **17**, 4939 (2005).
43. A. M. Nowak and R. L. McCreery, *Anal. Chem.* **76**, 1089 (2004).
44. S. Donner, H. W. Li, E. S. Yeung, and M. D. Porter, *Anal. Chem.* **78**, 2816 (2006).
45. S. Ranganathan and R. L. McCreery, *Anal. Chem.* **73**, 893 (2001).
46. S. Ranganathan, R. L. McCreery, S. M. Majji, and M. Madou, *J. Electrochem. Soc.* **147**, 277 (2000).
47. Y.-C. Liu and R. L. McCreery, *J. Am. Chem. Soc.* **117**, 11254 (1995).
48. F. Anariba, S. H. DuVall, and R. L. McCreery, *Anal. Chem.* **75**, 3837 (2003).
49. C. Combellas, F. Kanoufi, J. Pinson, and F. Podvorica, *Langmuir* **21**, 280 (2005).
50. J. K. Kariuki and M. T. McDermott, *Langmuir* **15**, 6534 (1999).
51. J. Pinson and F. Podvorica, *Chem. Soc. Rev.* **34**, 429 (2005).
52. M. J. Frisch, G. W. Trucks, H. B. Schlegel, G. E. Scuseria, M. A. Robb, J. R. Cheeseman, V. G. Zakrzewski, J. A. Montgomery, R. E. Stratmann, J. C. Burant, S. Dapprich, J. M. Millam, A. D. Daniels, K. N. Kudin, M. C. Strain, O. Farkas, J. Tomasi, V. Barone, M. Cossi, R. Cammi, B. Mennucci, C. Pomelli, C. Adamo, S. Clifford, J. Ochterski, G. A. Petersson, P. Y. Ayala, Q. Cui, K. Morokuma, D. K. Malick, A. D. Rabuck, K. Raghavachari, J. B. Foresman, J. Cioslowski, J. V. Ortiz, A. G. Baboul, B. B. Stefanov, G. Liu, A. Liashenko, P. Piskorz, I. Komaromi, R. Gomperts, R. L. Martin, D. J. Fox, T. Keith, M. A. Al-Laham, C. Y. Peng, A. Nanayakkara, C. Gonzalez, M. Challacombe, P. M. W. Gill, B. Johnson, W. Chen, M. W. Wong, J. L. Andres, C. Gonzalez, M. Head-Gordon, E. S. Replogle, and J. A. Pople, *Gaussian* (Gaussian, Inc., Pittsburgh, 1998), 7 ed.
53. M. W. Williams and E. T. Arakawa, *J. Appl. Phys.* **43**, 3460 (1972).
54. H. Liang, H. Tian, and R. McCreery, *Appl. Spectrosc.* **61**, 613 (2007).
55. J. Ouyang and A. B. P. Lever, *J. Phys. Chem.* **95**, 2101 (1991).
56. D. D. Schlereth and H.-L. Schmidt, *J. Electroanal. Chem.* **380**, 117 (1995).
57. S. Sortino, S. D. Bella, S. Conoci, S. Petralia, M. Tomasulo, E. J. Palsial, and F. M. Raymo, *Adv. Mater.* **17**, 1390 (2005).
58. V. Ruiz, A. Colina, M. A. Heras, and J. López-Palacios, *Small* **2**, 56 (2006).
59. V. Ruiz, A. Colina, M. A. Heras, and J. López-Palacios, *J. Phys. Chem. C* **111**, 4277 (2007).